

Standing torsional Alfvén waves as the source of the rotational period variation in magnetic early-type stars

Koh Takahashi^{1,2}, Norbert Langer^{3,4}

¹ National Observatory of Japan, National Institutes for Natural Science, 2-21-1 Osawa, Mitaka, Tokyo 181-8588, Japan
e-mail: koh.takahashi@nao.ac.jp

² Astronomical Institute, Tohoku University, 6-3 Aramaki Aza-Aoba, Aoba, Sendai, Miyagi 980-8578, Japan

³ Argelander-Institut für Astronomie, Universität Bonn, Auf dem Hügel 71, 53121 Bonn, Germany

⁴ Max-Planck-Institut für Radioastronomie, Auf dem Hügel 69, 53121 Bonn, Germany

Date:–

ABSTRACT

Context. The influence of magnetic fields on stellar evolution remains unresolved. It has been proposed that if there is a large-scale magnetic field in the stellar interior, torsional Alfvén waves could arise, efficiently transporting angular momentum. In fact, the observed variations in the rotation periods of some magnetic stars may be attributed to these torsional Alfvén waves' standing waves.

Aims. To demonstrate the existence of torsional Alfvén waves through modeling of the rotational period variations.

Methods. We conduct an eigenmode analysis of standing Alfvén waves based on one-dimensional magnetohydrodynamic equations. The internal magnetic field structures are parametrically represented to treat poloidal fields with different degrees of central/surface concentration. The obtained frequencies are compared with the observed frequencies of the rotational period variations, thereby constraining the internal magnetic field structures.

Results. The 67.6 years exhibited by CU Vir is reproduced for surface-concentrated magnetic field structures. The rotational period variations of all ten magnetic stars analyzed in this study are inconsistent with a centrally concentrated magnetic field.

Conclusions. Torsional Alfvén waves can reproduce the observations of rotational period variations. The large-scale magnetic fields within magnetic stars would be concentrated on the surface.

Key words. magnetohydrodynamics (MHD)—stars: chemically peculiar—stars: early-type—stars: magnetic field—stars: rotation

1. Introduction

About 10% of early-type (O-, B-, and A-type) stars are known to possess surface magnetic fields of the order of 100–10,000 G (Babcock 1958; Landstreet 1992; Wade et al. 2014; Keszthelyi 2023). In contrast to low-mass stars including the sun, the magnetic fields in these massive stars have a large-scale, time-stable structure. These properties support the idea that magnetic early-type stars possess a "fossil field", i.e., a magnetic field in mechanical equilibrium with the stellar plasma (Braithwaite & Spruit 2017). These stars are discussed as progenitors of compact objects with strong magnetic fields (e.g., Ferrario & Wickramasinghe 2006).

Several processes have been proposed through which magnetic fields may influence stellar evolution. If the magnetic energy density exceeds the internal energy density, magnetic pressure and tension can change the pressure and density structure of the star (Feiden & Chaboyer 2012, 2013, 2014). Even if it were not so strong, it could affect convection, meridional circulation, and rotationally induced flows with relatively small energy densities (e.g., Petermann et al. 2015). Several studies investigated the effect of magnetic stress onto the rotational evolution. External magnetic fields may exert torques on the stellar surface, braking its rotation (Weber & Davis 1967; Meynet et al. 2011; Petit et al. 2017; Georgy et al. 2017; Keszthelyi et al. 2019). Similarly, the magnetic field inside the star likely causes angular momentum transport and affects the rotation distribution (Spruit

1999, 2002; Heger et al. 2005; Wheeler et al. 2015; Fuller et al. 2019; Griffiths et al. 2022).

There also have been attempts to calculate the temporal evolution of the global magnetic field within magnetic stars (Potter et al. 2012; Takahashi & Langer 2021). The latter devised a formulation that satisfies conservation laws. If there is a poloidal (component within the meridional plane) magnetic field within a rotating star, the differential rotation stretches it and induces a toroidal (component winding around the magnetic axis) component. As a result, a magnetic torque is induced which drives waves of angular momentum through the poloidal magnetic field: torsional Alfvén waves. Takahashi & Langer (2021) discovered that the propagation of the dissipating torsional Alfvén waves redistributes angular momentum efficiently inside the star, providing an explanation for the slow rotation of the cores of red giants (Beck et al. 2012; Mosser et al. 2012; Deheuvels et al. 2014).

Therefore, the question of whether there is a large-scale magnetic field inside a star is crucial because it can affect the overall stellar evolution. While observational evidence has verified the presence of a global magnetic field on the surface of magnetic stars, how this field is distributed and connected within the stellar interior remains unexplored. Asteroseismic analyses have suggested the presence of strong magnetic fields within the interiors of stars (Fuller et al. 2015; Stello et al. 2016), and more quantitative estimates have been made recently (for B-type main-sequence stars: Lecoanet et al. 2022; for red giants: Li et al. 2022, 2023). However, current magnetic field detections via as-

teroseismology are sensitive to only a narrow region within the stellar interior (the core surface), and the global structure remains largely unconstrained.

In this work, we focus on the intriguing phenomenon observed in some hot magnetic stars regarding their rotational periods to address the issue. A- and B-type stars with magnetic fields are known to exhibit chemical peculiarities in their spectra, leading to their classification as Ap/Bp stars (Maury & Pickering 1897; Lockyer & Baxandall 1906; Morgan 1933; Preston 1974). It was already noted in the early 1900s that these peculiar lines show time variation (Lockyer & Baxandall 1906; Ludendorff 1906), and later, its periodic nature with a period of 5.5 days was demonstrated for α^2 CVn, known today as a typical Ap star (Belopolsky 1913). Concurrently, a periodic variation in the stellar luminosity was also discovered, and it was shown that this period matches the spectroscopically determined period (Guthnick & Prager 1914).

After the detection of surface magnetic fields on 78 Vir (Babcock 1947b), the strength of the magnetic field (Babcock 1947a, 1948), line intensities (Morgan 1931, 1933; Deutsch 1947), and the luminosity (Stibbs 1950) of CU Vir were all found to vary synchronously. This variation of multiple quantities with a single period is currently explained with the Oblique Rotator Model, which assumes that the magnetic field symmetry axis is inclined to the rotation axis of the magnetic stars (Babcock 1949; Stibbs 1950; Deutsch 1954, 1958; Wolff 1983).

Due to this historical background, there exist long-term, high-precision observations of the rotation periods for some magnetic stars. Such an extended monitoring allows observers to discover changes of the rotation periods occurring over timescales of several decades. Such changes were initially detected through phase shifts in light curves (56 Ari in Adelman & Fried 1991; CU Vir in Adelman et al. 1992). Subsequently, Pyper et al. (1998) introduced the O-C analysis and accurately confirmed the phase shifts for CU Vir. Entering the 2000s, not only stars with increasing rotation periods, which indicate a deceleration in rotation velocity (Reiners et al. 2000; Mikulášek et al. 2008; Townsend et al. 2010), but also stars showing decreasing rotation periods, suggesting accelerating rotation (Ozuyar & Stevens 2018; Shultz et al. 2019a; Pyper & Adelman 2020), were reported.

The rotational period variations discussed above indicate either a steady deceleration or acceleration in rotation, which corresponds to the first time derivative of the rotation period. Even more exciting, for CU Vir and V901 Ori, the presence of both, deceleration and acceleration phases, were indicated in the long-term evolution of the rotation period (Mikulášek et al. 2011). Additionally, V913 Sco, indicating an acceleration, may also exhibit a non-zero second derivative of the rotation period (Shultz et al. 2019a). The presence of accelerating and decelerating stars, and even the coexistence of both phenomena in a single star, may suggest that the cyclic variations in rotation periods are a universal phenomenon among hot magnetic stars (Mikulášek et al. 2022).

Various explanations for the origin of rotational period variations have been proposed. Shore & Adelman (1976) predicted that stars with magnetic fields, due to their non-spherical distortion, would undergo free or forced precession in cases of single or binary stars, respectively. According to the Oblique Rotator Model, a precessing magnetic star should alter the shape of its light curve, as well as shift phases of maximum and minimum light by changing the line-of-sight direction. Observational evidence has been obtained in several magnetic stars, including 56 Ari (Adelman & Fried 1991; Ziznovsky et al. 2000; Pyper &

Adelman 2021). However, explaining stars like CU Vir, which exhibit rotational period variations while maintaining the shape of their light curves, is challenging to understand with precession alone (Mikulášek et al. 2011). Magnetic braking, resulting from the coupling between stellar winds and surface magnetic fields, can also cause rotational period variations. This process is expected in high-mass stars and may explain the deceleration of rotation in magnetic OB stars like σ Ori E (Townsend et al. 2010). However, its occurrence in relatively low-mass magnetic stars is uncertain, and explaining acceleration poses challenges. Other hypotheses such as migrating spots and mass accretion have been considered (Adelman et al. 1992; Pyper et al. 1998), but whether these scenarios can explain the deceleration or acceleration observed over decades-long timescales remains uncertain.

Although the mechanism of rotational period variation is not yet understood, the global magnetic field of the stellar interior may be of relevance. Stępień (1998) speculated that the coupling between the magnetic field and the meridional circulation in the stellar envelope may be responsible for the rotational period variation. Krtička et al. (2017) further elaborated on this idea and attempted to explain the rotational period variation by standing torsional Alfvén waves. They assumed a goblet-like poloidal magnetic field penetrating the stellar interior, and they considered the torsional Alfvén waves by solving a one-dimensional induction equation. Giving the modulating rotation as a boundary condition, they scanned the frequencies corresponding to the standing waves. They found that the fundamental mode frequency corresponds well to the frequency of the rotational period variation observed for CU Vir. Although their model could not explain V901 Ori, they demonstrated that standing Alfvén waves have the potential to explain rotational period variation.

In this study, the properties of standing Alfvén waves in magnetic stars are investigated in more detail, based on the method developed by Takahashi & Langer (2021). This method decomposes the large-scale magnetic field inside a star into poloidal and toroidal components, each of which can have an arbitrary radial dependence. It allows us to investigate the dependence of the variation period on the poloidal field geometry, beyond those considered in Krtička et al. (2017).

The magnetic field structures considered here are still very simplified, and not capable of fully capturing the complex structures found in real stellar magnetospheres. Therefore, a quantitative comparison between theory and observation may not be very meaningful. Instead, we seek to qualitatively investigate which properties significantly affect the timescale of variability. Ultimately, we aim to test the existence of torsional Alfvén waves and establish a picture of angular momentum transport in the stellar interior by large-scale magnetic fields through a comparison of predicted variations of the rotational period with observations.

In the next section, we compile the available observational constraints and explain our strategy for predicting the rotational period variation by internal Alfvén waves. In Section 3, after analyzing the properties of standing torsional Alfvén waves using CU Vir as an example, we will derive constraints for the internal magnetic field structure of ten magnetic stars. In Section 4, we discuss the limitations of this model, its relation to previous research on the internal magnetic field structures of stars, the excitation mechanisms of torsional waves, and the prospects for future detection of rotational period variation. We summarize concluding remarks in Section 5.

2. Method

2.1. Magnetic stars that show rotational period variations

In this study, we analyzed ten magnetic stars that exhibit variations in their rotation periods. These stars are listed in Table 1, which displays their parameters, including surface effective temperature, luminosity, and the strength of the magnetic field at the pole. These values are collected from the literature that is indicated by the footnote of the table. As we could not find spectroscopic values for 13 And, a photometric estimate has been done using the B and V band magnitudes listed in SIMBAD ($m_B=5.726$, $m_V=736$) with a bolometric correction (Cox 2000) and a parallax of 10.3618 mas. The uncertainty is roughly estimated based on the errors of photometric values relative to their spectroscopic values for other listed stars. Also, for V343 Pup, 13 And, V473 Tau, and BS Cir, we couldn't find literature indicating their surface magnetic field strength, so we assumed a typical value of 1 kG. To detect rotational period variations, it is essential to have extended, regular monitoring of the rotation period over the long term. Hence, the table includes the length of the monitoring period, T_{baseline} , for each magnetic star. The time derivative of the rotation periods, which is the direct observational indication of the rotational period variation, is also shown.

An increase in the rotation period, indicating a deceleration in rotational velocity, was detected from σ Ori E (Townsend et al. 2010; Mikulášek 2016), V901 Ori (Mikulášek et al. 2008, 2011; Mikulášek 2016; Pyper & Adelman 2020), 56 Ari (Adelman & Fried 1991; Adelman et al. 2001), V343 Pup (Mikulášek et al. 2022), BS Cir (Mikulášek 2016), and CS Vir (Ozuyar et al. 2018, but see Pyper & Adelman 2020). On the other hand, V913 Sco (Shultz et al. 2019a; Pyper & Adelman 2020), 13 And (Pyper & Adelman 2020), and V473 Tau (Ozuyar & Stevens 2018) exhibit a decrease in the rotation period, implying an acceleration in their rotational velocities. Furthermore, CU Vir exhibits a transition in its rotational period variation from increasing to decreasing (Adelman et al. 1992; Pyper et al. 1998; Mikulášek et al. 2011; Mikulášek 2016, but for alternative interpretation, see Pyper & Adelman 2020), suggesting the possibility of cyclic nature of the variation. While different authors have reached different conclusions, the change of the sign of the rotational period variations may also occur for V901 Ori (Mikulášek 2016) and V913 Sco (Shultz et al. 2019a). The cyclic changes in the rotational period variation take place on timescales of several decades, with estimated periods of 67.6 years for CU Vir, 60 years for V913 Sco, and more than 100 years for V901 Ori.

We prepare a set of nonrotating, nonmagnetic stellar evolution simulations using the stellar evolution code HOSHI (Takahashi & Langer 2021). The results are compared to the magnetic stars on the HR diagram, which is shown as Fig. 1. This allows us to select the best-fit models to determine each object's zero-age main-sequence (ZAMS) mass and age, which are indicated in the table. The stars' ages are presented both as mega-years and as fractional ages normalized to the duration of the main sequence stage. While magnetic fields and rotation may exert considerable influences on tracks in the HR diagram (Petermann et al. 2015; Keszhelyi et al. 2019, 2020), their effects are not essential for the scope of this study.

We searched the literature for indications of these stars belonging to clusters or associations. σ Ori E is thought to belong to the σ Orionis Open Cluster (e.g., Tarricq et al. 2021), which is estimated to be 3–5 Myr old (Zapatero Osorio et al. 2002). V901 Ori is suggested to belong to the Ori B star-forming region, which has an age of 0.8–2.2 Myr (Román-Zúñiga et al.

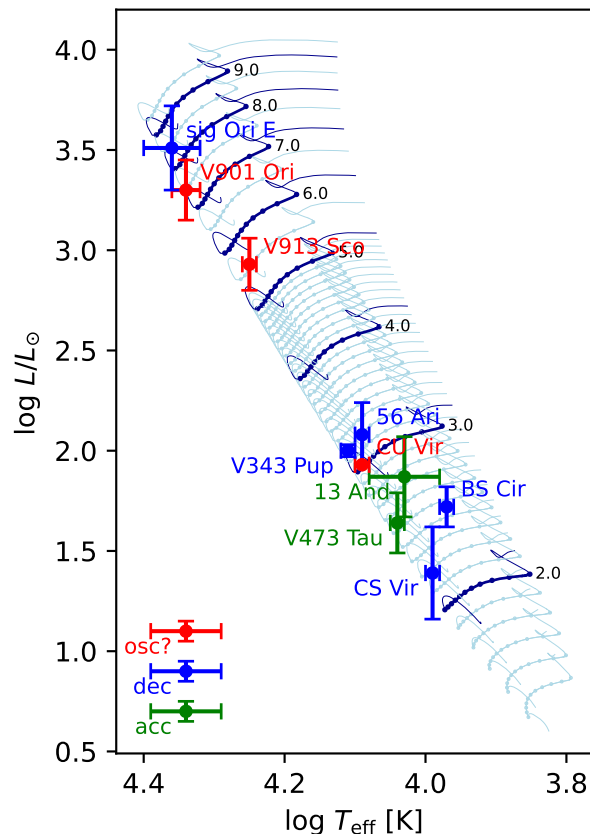


Fig. 1. The ten magnetic stars where rotational period variations have been detected are shown on the HR diagram. Those showing a long-term increase in rotation period are represented in blue (decelerating), those with a decrease in green (accelerating), and those transitioning from an increase to a decrease (or vice versa) in red (oscillating). The solid curves represent the results of evolution calculations of nonrotating, nonmagnetic stars. Models with ZAMS masses from 1.5 to 5 M_{\odot} are shown at intervals of 0.1 M_{\odot} , while models with ZAMS masses from 5.5 to 9.5 M_{\odot} are shown at intervals of 0.5 M_{\odot} . The numbers displayed next to the solid curves represent the ZAMS mass. To indicate the ages, points were placed at 10 equal divisions of the period from ZAMS to TAMS.

2023), while V913 Sco may be part of Upper Sco with an age of 10–12 Myr (Esplin et al. 2018; Luhman & Esplin 2020). V343 Pup is also thought to belong to the Vela OB2 complex (Cantat-Gaudin et al. 2019). The age of this association is estimated to be 7.5–10 Myr from isochrones, which is somewhat inconsistent with the lithium depletion observed in pre-main-sequence stars (Prisinzano et al. 2016; Jeffries et al. 2017). While the estimated ages for the parent regions do not perfectly match our age estimates, no significant discrepancies are found due to the large uncertainties in our estimates. We do not find works suggesting relationships with known clusters and associations for the other stars in our sample.

2.2. Stellar models

The HOSHI code we used to compute stellar models is a general-purpose stellar evolution code designed to handle standard physics such as radiative and convective energy transfer, time-dependent chemical mixing, nuclear reactions, as well as stellar rotation and stellar magnetism. Here we briefly describe the most relevant elements of the code, the treatment of rota-

Table 1. A list of magnetic stars that show rotational period variations.

| Object | HD | $\log T_{\text{eff}}$ K | $\log L/L_{\odot}$ | B_{pole} kG | P_{rot} d | T_{baseline} yr | dP_{rot}/dt $10^{-2} \text{ s yr}^{-1}$ | M_{ini} M_{\odot} | τ Myr | τ/τ_{MS} |
|----------------|--------|----------------------------|--------------------|-------------------------|-----------------------|-----------------------------|---|---------------------------------|---------------|-------------------------|
| σ Ori E | 37479 | 4.361 ± 0.039^a | 3.51 ± 0.21^a | $7.55^{+0.25b}_{-0.25}$ | 1.191^a | 43 (1974–2017) ^c | 9.71 ± 0.09^c | 8.5 | 4.33 | 0.1 |
| V901 Ori | 37776 | 4.342 ± 0.019^a | 3.30 ± 0.15^a | $6.1^{+0.7a}_{-0.7}$ | 1.539^a | 36 (1977–2013) ^d | 35.3 ± 0.9^c | 7.5 | 0.00 | 0.0 |
| V913 Sco | 142990 | 4.255 ± 0.012^a | 2.93 ± 0.13^a | $4.7^{+0.4a}_{-0.4}$ | 0.979^a | 39 (1976–2015) ^e | -58 ± 1^e | 5.5 | 27.6 | 0.3 |
| 56 Ari | 19832 | 4.093 ± 0.013^a | 2.08 ± 0.16^a | $2.7^{+0.6a}_{-0.3}$ | 0.728^a | 48 (1952–2001) ^f | 2.25^f | 3.2 | 196 | 0.6 |
| V343 Pup | 60431 | 4.114 ± 0.01^g | 2.00 ± 0.032^g | - | 0.476^g | 35 (1986–2021) ^g | 0.74 ± 0.05^g | 3.2 | 45.1 | 0.1 |
| CU Vir | 124224 | 4.089 ± 0.003^a | 1.93 ± 0.01^a | $4.0^{+0.2h}_{-0.2}$ | 0.521^a | 67 (1949–2016) ^c | 8.817 ± 12^c | 3.0 | 54.5 | 0.1 |
| 13 And | 220885 | 4.03 ± 0.05^i | 1.87 ± 0.2^i | - | 1.479^d | 23 (1990–2013) ^d | -63.4^d | 2.7 | 306 | 0.6 |
| V473 Tau | 30466 | 4.045 ± 0.011^j | 1.64 ± 0.15^j | - | 1.407^j | 47 (1963–2010) ^j | -11 ± 3^j | 2.5 | 71.9 | 0.1 |
| BS Cir | 125630 | 3.966 ± 0.014^k | 1.72 ± 0.10^k | - | 2.204^c | 39 (1975–2014) ^c | 17.0 ± 1.3^c | 2.5 | 493 | 0.8 |
| CS Vir | 125248 | 3.992 ± 0.013^a | 1.50 ± 0.08^a | $9.0^{+1.1a}_{-1.3}$ | 9.300^a | 83 (1928–2011) ^l | 66 ± 8^l | 2.2 | 184 | 0.2 |

Notes. Columns: T_{eff} , L , and B_{pole} are the effective temperature, the luminosity, and the magnetic field strength at the magnetic pole, respectively. T_{baseline} is the baseline duration of the observations for rotational periods. M_{ini} , τ , and τ/τ_{MS} are the initial mass, the age, and the main-sequence fractional age, respectively, that are estimated theoretically via fitting to the location in the HR diagram. References: ^(a) Shultz et al. (2022) ^(b) Oksala et al. (2015) ^(c) Mikulášek (2016) ^(d) Pypser & Adelman (2020) ^(e) Shultz et al. (2019a) ^(f) Adelman et al. (2001) ^(g) Mikulášek et al. (2022) ^(h) Kochukhov et al. (2014) ⁽ⁱ⁾ SIMBAD photometry ^(j) Ozuyar & Stevens (2018) ^(k) Kochukhov & Bagnulo (2006) ^(l) Ozuyar et al. (2018)

tion and magnetic fields, and a more detailed description can be found in Takahashi & Langer (2021).

The code uses angular velocity as one of the independent variable to treat stellar rotation. As a critical assumption, our formulation treats that the angular velocity of the gas can be expressed as a function of the enclosed mass $\Omega(M)$. This relies on the assumption known as the ‘shellular rotation law’ (Zahn 1992), which adopts a picture where viscosity due to horizontal turbulence homogenizes the angular velocity on equipressure surfaces. The validity of this assumption will be discussed later.

The time evolution of the angular velocity distribution is determined by the following diffusion equation with an additional term that shows magnetic stress:

$$\frac{d}{dt}(i\Omega) = \frac{\partial}{\partial M} \left((4\pi\rho r^2)^2 v_{\text{cv}} i r^{-n_{\text{cv}}} \frac{\partial(\Omega r^{n_{\text{cv}}})}{\partial M} \right) + \frac{\partial}{\partial M} \left((4\pi\rho r^2)^2 v_{\text{eff}} i \frac{\partial\Omega}{\partial M} \right) + \frac{\partial}{\partial M} \left(\frac{8r^2 AB}{15} \right), \quad (1)$$

where i , ρ , r , A , and B are the specific moment of inertia, density, radius, toroidal vector potential expressing poloidal magnetic component, and toroidal magnetic component, respectively, all of which are functions of mass. v_{cv} is the viscosity due to convective turbulence and is estimated as $v_{\text{cv}} = v_{\text{cv}} l_{\text{cv}}/3$ using the convective velocity v_{cv} and length scale l_{cv} provided by the mixing-length theory. A fudge factor n_{cv} is introduced to absorb our ignorance of angular momentum transport due to convective turbulence. In this work, $n_{\text{cv}} = 0$ is used so that convective regions rotate rigidly. v_{eff} is the effective viscosity due to turbulence caused by instabilities other than convection. The dynamical and secular shear instability, the Solberg-Hoiland instability, and the Goldreich-Schubert-Fricke instability are included here as instabilities due to rotation (Pinsonneault et al. 1989; Heger et al. 2000), and the Pitts-Tayler instability as instability due to magnetic fields (Spruit 2002; Maeder & Meynet 2004). The boundary condition is to set all angular momentum fluxes to zero at the inner and outer boundaries.

The evolution of the stellar magnetic field is represented by the time evolution of two functions, $A(M)$ for the poloidal component and $B(M)$ for the toroidal component:

$$\frac{d}{dt}(Ar) = 4\pi\rho\eta r^3 \frac{\partial}{\partial M} \left(4\pi\rho \frac{\partial(Ar^2)}{\partial M} \right), \quad (2)$$

$$\frac{d}{dt} \left(\frac{B}{\rho r} \right) = 4\pi Ar \frac{\partial\Omega}{\partial M} + 4\pi\eta r^2 \frac{\partial}{\partial M} \left(\frac{4\pi\rho}{r^2} \frac{\partial(Br^3)}{\partial M} \right) + (4\pi)^2 \rho r^2 \frac{\partial\eta}{\partial M} \frac{\partial(Br)}{\partial M}. \quad (3)$$

η represents the effective magnetic viscosity. It is estimated as $\eta = v_{\text{cv}} + f_m \times v_{\text{eff}}$ with a parameter f_m . The control parameter f_m is introduced to handle the large uncertainty of the turbulent transport coefficients, but $f_m = 1$ is used in this study. The inner boundary conditions are chosen as $\partial(A/r)/\partial M = 0$ and $\partial(B/r^2)/\partial M = 0$ so that the magnetic fields do not diverge and are smoothly connected to the solution of the diffusion equations at the center. At the stellar surface, we assume that the poloidal component smoothly connects to the external dipole field, and the toroidal component is set to zero because the electric current is assumed not to penetrate the stellar surface. These are expressed by $\partial(Ar^2)/\partial M = 0$ and $B = 0$.

2.3. The eigenmode analysis

Takahashi & Langer (2021) showed that the eqs. 1 and 3 can be reduced to a wave equation representing the propagation of torsional Alfvén waves if the time evolution of density, radius, poloidal magnetic component and other coefficients are negligible. This means that the standing waves of the torsional Alfvén wave of interest in this study can be expressed as eigenmodes of this wave equation. Therefore, we conduct an eigenmode analysis to find standing-wave solutions instead of directly solving the wave propagation and scanning the frequency space as done in Krtićka et al. (2017). With this method, each eigenmode, including higher-order modes can be efficiently and robustly obtained. It has been confirmed that the obtained eigenmodes describe oscillatory time evolution by actually solving the dynamical evolution for several models.

The independent variables of the wave equation are $\Omega(t, M)$ and $B(t, M)$, and it can be schematically expressed as

$$\begin{aligned} \frac{\partial\Omega}{\partial t} &= F_{\Omega}(\Omega, B) \\ \frac{\partial B}{\partial t} &= F_B(\Omega, B). \end{aligned} \quad (4)$$

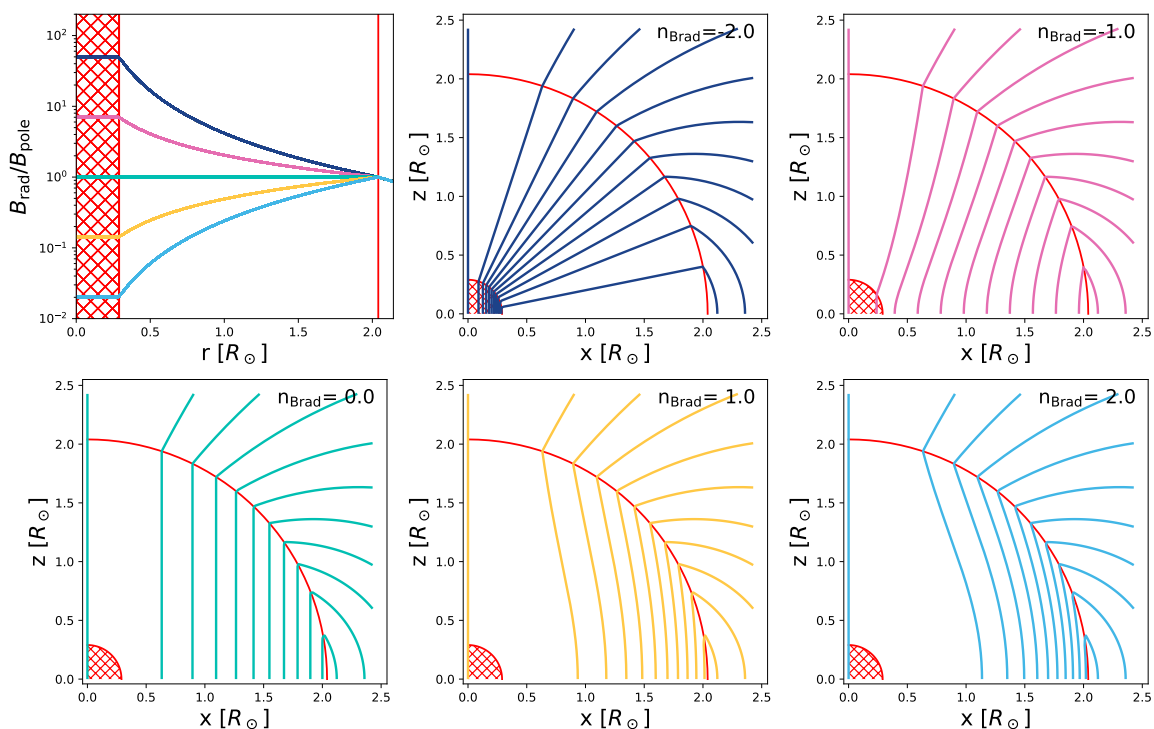


Fig. 2. The examples of parametric poloidal field structures that are applied in this work. Solid lines in the top-left panel show the radial dependencies of $B_{\text{rad}}/B_{\text{pole}}(r)$ functions with $n_{\text{Brad}} = -2.0$ (dark blue), -1.0 (magenta), $+0.0$ (green), $+1.0$ (yellow), and $+2.0$ (cyan). The red-hatched region in the stellar center corresponds to the central convective region, in which the magnetic field is assumed to be constant. The vertical red-solid line indicates the stellar surface, where $B_{\text{rad}}/B_{\text{pole}}(r) = 1$. The rest plots show the 2D poloidal field structures in the meridional cuts. As in the top-left panel, the red-hatched area shows the central convective region and the red-solid curve is the stellar surface.

Here, F_{Ω} and F_B are terms expressing the advection and diffusion in eqs. 1 and 3. They are partial derivatives in the original equations, but in numerical calculations, they are expressed as linear functions of the Ω and B vectors. Hence, if we assume that the two independent variables have a common time dependence of $\Omega \sim B \sim \exp(\lambda t)$, it is further reduced to a linear equation as

$$\lambda \mathbf{x} = F \cdot \mathbf{x}, \quad (5)$$

where $\mathbf{x} = (\Omega, B)^T$ is a vector arranging the independent variables in a row, and F is a matrix showing the advection and diffusion terms. Eq. 4 indeed forms an eigenvalue problem of the matrix F with the eigenvalue of λ and the associated eigenvector of \mathbf{x} .

The eigenvalue λ is decomposed into the real part σ and the imaginary part ω ,

$$\lambda = \sigma + i\omega,$$

where i in this equation shows the imaginary unit, and a non-zero imaginary part means that the eigenmode shows an oscillatory evolution. We interpret this oscillatory evolution as the rotational period variation observed in some magnetic stars. Hence, the period of the variation, Π , can be estimated as $\Pi = 2\pi/\omega$ using the eigenvalue in this model. We will investigate the properties of Π later on. One of the limitation of this model is that, since it is based on a linear analysis, it cannot predict the amplitude of the rotational period variation, which requires some kind of driving mechanism that is beyond the scope of the present study.

In practice, we evaluate the matrix F from partial derivatives of F_{Ω} and F_B as

$$F = \begin{pmatrix} \frac{\partial F_{\Omega}}{\partial \Omega} & \frac{\partial F_{\Omega}}{\partial B} \\ \frac{\partial F_B}{\partial \Omega} & \frac{\partial F_B}{\partial B} \end{pmatrix}$$

since they are already prepared to form the Jacobian in the main Newton-Raphson iteration for evolution simulations. Hence, our eigenmode analysis shares the spacial resolution with the stellar evolution simulation. The mesh number is typically ~ 1000 . Both F_{Ω} and F_B actually include nonlinear terms of Ω and B in the diffusion coefficients, which we assume to be negligible. This assumption seems reasonable, since the direct simulation of the time evolution with the obtained eigenmodes as input reproduced the standing waves very well. The eigenmode analysis of the F matrix is done using the DGEEV subroutine in the open library LAPACK.

2.3.1. The parametric structure of the poloidal magnetic field

The magnetic field structure of stellar interiors remains a perplexing subject. In this study, the strategy is to describe the internal structure of the poloidal magnetic field using a simple parametric function with minimal assumptions. First, the magnetic field is assumed to be axisymmetric to the axis of rotation, as in the basic definition of our evolution simulation. Second, the

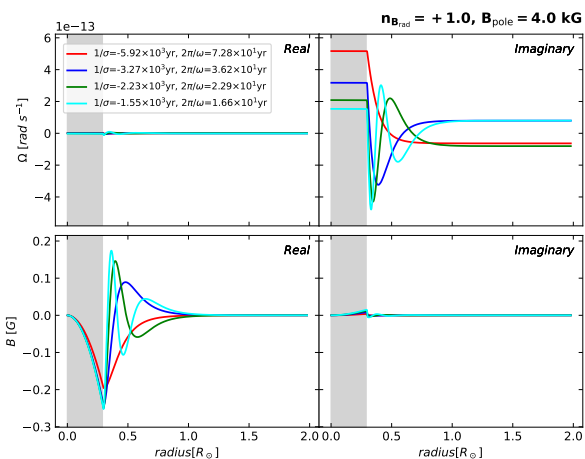


Fig. 3. Eigenfunctions obtained for the CU Vir model with $n_{\text{Brad}} = +1.0$. The top two panels display the distribution of angular velocity, $\Omega(r)$, while the bottom two panels show the toroidal magnetic field component, $B(r)$. In each row, the left panel shows the real part, and the right panel shows the imaginary part. The modes from the lowest to the fourth are indicated as red, blue, green, and cyan lines. The reciprocals of the eigenvalues for each mode are shown in the legend. The gray-shaded area indicates the central convective region.

radial dependence is expressed using the parameter n_{Brad} as

$$B_{\text{rad}}(r) = B_{\text{pole}} \times \begin{cases} (R_{\text{cv}}/R_{\text{star}})^{n_{\text{Brad}}} & (r < R_{\text{cv}}) \\ (r/R_{\text{star}})^{n_{\text{Brad}}} & (r > R_{\text{cv}}), \end{cases} \quad (6)$$

where R_{cv} and R_{star} are the radius of the central convective region and the stellar radius and B_{pole} is the magnetic flux density at the pole on the stellar surface. The magnetic stars considered in this work are early-type main-sequence stars, and all of them have a convective region in the center. Therefore, the magnetic field does not diverge or go to zero at the center using this expression. Then, the radial field is converted into the A function as $A = B_{\text{rad}} \times r/2$. Figure 2 shows magnetic field structures with different n_{Brad} applied to the CU Vir model as an example.

2.3.2. A correlation between Π and B_{pole}

As noted in Krtička et al. (2017), the eigenvalue λ follows a scaling transformation of $\lambda' = \gamma^{-1}\lambda$ with $B'_{\text{pole}} = \gamma B_{\text{pole}}$ due to the linear dependence of the matrix F on B_{pole} . Hence, a linear relationship between Π and B_{pole} can be obtained:

$$\Pi \times B_{\text{pole}} = \text{const}. \quad (7)$$

One may calculate Π for models with different values of B_{pole} using this relationship. Furthermore, the uncertainty in B_{pole} is associated with the uncertainty in Π through this relationship.

3. Results

3.1. General trends of the eigenmode analysis

First, we discuss the general trends of the eigenmode analysis by taking the CU Vir model as an example. The background structure is taken from a model with $M_{\text{ini}} = 3.0 M_{\odot}$ and $\tau = 54.5$ Myr. In Fig. 3, lowest-order eigenmodes from the first to the fourth obtained for the model with $n_{\text{Brad}} = +1.0$ are shown as a function of radius. In the central convective region, Ω profiles become flat

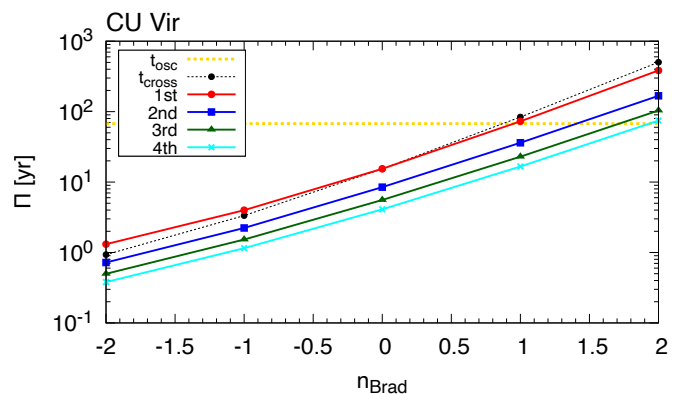


Fig. 4. The n_{Brad} dependence of oscillation periods estimated for the CU Vir model is shown for eigenfunctions from the first to the fourth orders. Different line styles are used for first (red, circle), second (blue, square), third (green, triangle), and fourth (cyan, cross). For comparison, t_{cross} is indicated by a black dotted line. The constant value shown as a yellow dashed line corresponds to the oscillation period suggested for CU Vir (67.6 yr).

and $B(r)$ profiles become $\propto r^2$ due to the large diffusion coefficient. Outside the convective region, both profiles show characteristic oscillatory patterns, whose number of nodes corresponds to the order. For example, for the lowest order mode, the number of nodes in the Ω and B profiles are 1 and 0, respectively, and it increases by one as the order of the eigenmode increases. And the frequency of the torsional oscillation, $\Pi = 2\pi/\omega$, decreases as the order of the mode increases.

The n_{Brad} dependence of the period of torsional oscillation is shown in Fig. 4. With the observational constraint of $B_{\text{pole}} = 4.0$ kG for CU Vir (Kochukhov et al. 2014; Shultz et al. 2022), n_{Brad} becomes the only parameter left to specify the internal poloidal field structure in our formulation. The figure shows that the larger the value of n_{Brad} , the longer the oscillation periods irrespective to the order. Hence, there is a simple one-to-one relationship between the parameter n_{Brad} and the frequency of oscillations. This relationship indicates that, within a crude approximation of the internal B-field structure, the structure of the internal poloidal field can be inferred by observing the period of torsional oscillations. Specifically, there are long enough observations for CU Vir, indicating that the rotation period may oscillate with a period $\Pi = 67.6$ yr. This period can be explained as the fundamental mode of the torsional oscillation with $n_{\text{Brad}} \sim +1.0$, indicating that the internal B-field is slightly concentrated on the stellar surface, rather than the center, for this particular case.

The figure also shows that the frequency of the lowest-order, which is shown by the red solid line, agrees well with the crossing time of the torsional Alfvén wave, the black dotted line. The crossing time is estimated as

$$t_{\text{cross}} = \int_0^{R_{\text{star}}} \frac{dr}{c(r)}, \quad (8)$$

where $c = B_{\text{rad}} / \sqrt{20\pi\rho}$ is the characteristic speed of the torsional Alfvén wave in our formulation (Takahashi & Langer 2021). This equation indicates that the region with the slowest wave propagation speed dominates the overall crossing time. Additionally, the strength of the poloidal magnetic field is proportional to the wave propagation speed and inversely proportional to the crossing time. This gives a physical explanation of the relation eq. (7).

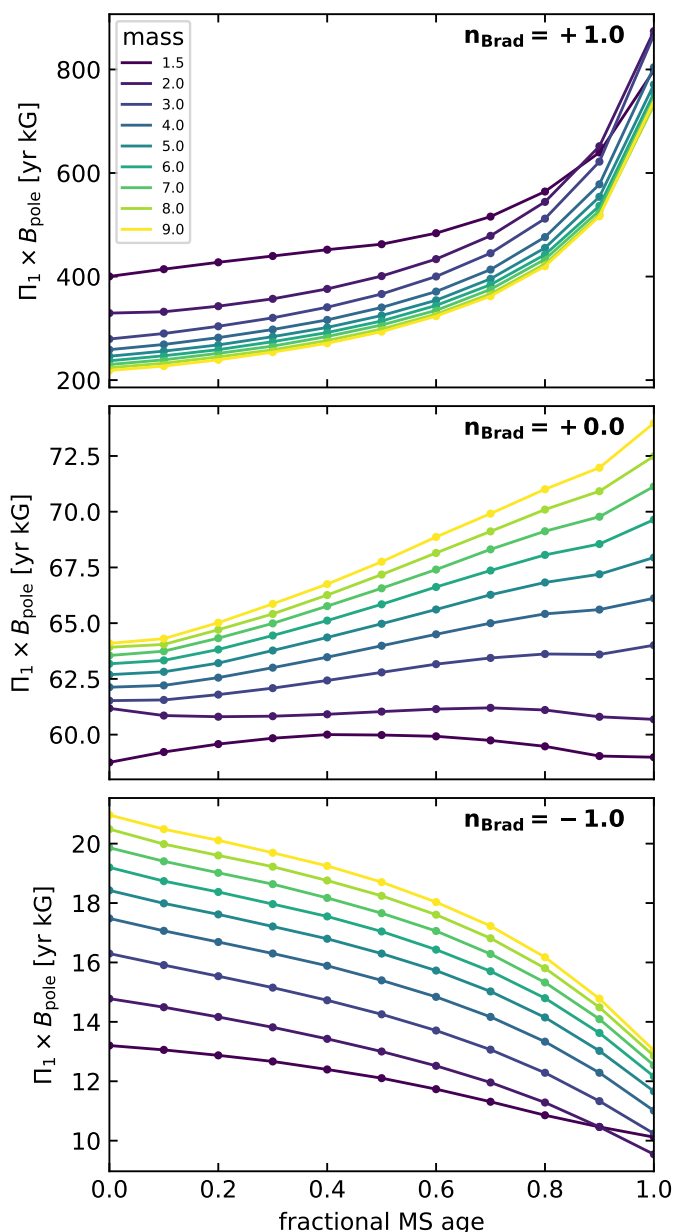


Fig. 5. Variation periods Π for different background structures with different fractional main-sequence ages and masses. Three panels show results with different n_{Brad} of +1.0 (top), +0.0 (middle), and -1.0 (bottom). The dependency on B_{pole} is implicitly included in the y-axis based on the relation eq.(7).

3.2. Variation periods with different background structures

The variation period Π depends not only on the magnetic field structure but also on the background density structure. Figure 5 illustrates how Π varies as the mass and age of the background structure model are changed while keeping the parameters specifying the magnetic field structure. It not only shows that Π depends on the background model, but also demonstrates how this dependency varies with n_{Brad} . Namely, for the case where the magnetic field is concentrated on the surface ($n_{\text{Brad}} = +1.0$), Π increases with increasing age and decreasing mass. Conversely,

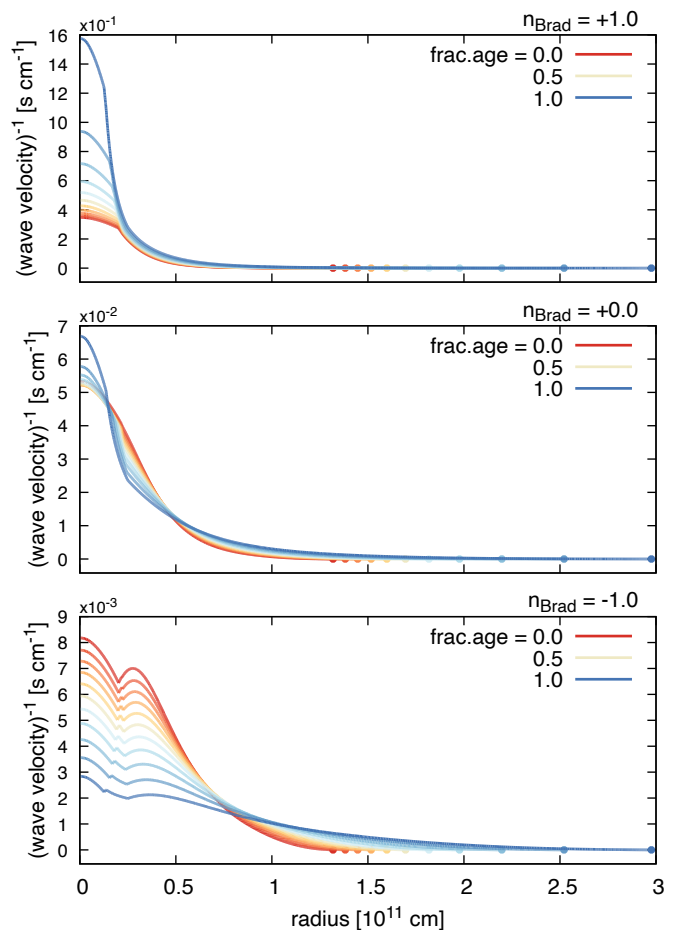


Fig. 6. The inverse of the velocity of torsional Alfvén wave is shown as a function of radius such that the enclosed area by the curves corresponds to the crossing time. From top to bottom, results for $n_{\text{Brad}} = +1.0, +0.0,$ and -1.0 with $B_{\text{pole}} = 1$ kG are shown. The density distributions are based on the $3 M_{\odot}$ model. Each panel includes 11 lines corresponding to different fractional MS ages of 0.0, 0.1, ..., 1.0, with the color of the lines changing from red to blue. Filled circles represent a change in radius.

for the case where the magnetic field is centrally concentrated ($n_{\text{Brad}} = +1.0$), the trend reverses, and Π increases with decreasing age and increasing mass. However, the change in Π due to differences in background structure remains at most a few times, which is relatively small compared to the change due to differences in n_{Brad} , which can span several orders of magnitude.

Different values of n_{Brad} lead to varying dependencies on the background, and most importantly, changing the value of Π significantly. This characteristic should be closely related to the velocity distribution of torsional Alfvén waves within the star, in particular, the distribution of propagation time in bottleneck regions. To explore this, the distribution of inverse of the Alfvén velocity is plotted in Fig. 6 for $M_{\text{ini}} = 3 M_{\odot}$ models with different ages. The top panel illustrates the results for $n_{\text{Brad}} = +1.0$, while the middle and bottom panels are for $n_{\text{Brad}} = +0.0$ and -1.0 , respectively. In this figure, the area enclosed by the lines and the x-axis corresponds to the crossing time.

The figure shows that the region where Alfvén waves slow down the most is the central part of the star, regardless of the magnetic field structure. This indicates that, even with $n_{\text{Brad}} = -1.0$, the increase in density at the center is responsible for de-

termining the speed of Alfvén waves. On the other hand, despite keeping the surface magnetic field strength constant, the speed of Alfvén waves changes by an order of magnitude with different $n_{\text{B,rad}}$. This is why the crossing time and Π show the large $n_{\text{B,rad}}$ dependence.

In the case of $n_{\text{B,rad}} = +0.0$, the wave velocity distribution remains relatively unchanged as the star ages. In this model, a uniform magnetic field of constant strength is imposed throughout the stellar interior, and the wave velocity is only affected by variations in the density distribution. Therefore, the time-constant nature indicates that changes in the density distribution during main-sequence star evolution itself do not have a significant impact on the oscillation period evolution. On the other hand, for $n_{\text{B,rad}} = \pm 1.0$, the changes in density distribution have a stronger impact on the variation period. This is because, when using our magnetic field structure description, the field strength in the central region directly depends on the stellar radius. The larger the age of the model, the larger the radius. Hence, in the case of $n_{\text{B,rad}} = +1.0$, the central magnetic field becomes weaker, causing the velocity to slow down. Conversely, for $n_{\text{B,rad}} = -1.0$, the central field becomes stronger, resulting in faster wave velocities. In other words, the change in the variation period with different ages can be attributed more to the simplification of the magnetic field structure used in this work rather than being a direct physical consequence of stellar evolution.

3.3. Eigenmode analysis for specific magnetic stars

The same analysis as conducted on CU Vir is applied to the other nine magnetic stars that are listed in Table 1, and the results are shown in Fig. 7 for all ten stars. To perform eigenmode analysis using our model, it is necessary to set the magnetic field strength on the stellar surface. As noted in section 2., we couldn't find such values for V343 Pup, 13 And, V473 Tau, and BS Cir, so a typical value of $B_{\text{pole}} = 1$ kG is applied for these stars. The obtained periods follow the relationship $\Pi \times B_{\text{pole}} = \text{const}$. Consequently, they may linearly shift up and down based on the actual field strength. To indicate this additional uncertainty, the results of the eigenvalues for the two stars are shown in dashed lines.

Detecting rotational period variations requires long-term monitoring, and for each star, the duration of this extended monitoring is indicated as T_{baseline} . It is expected that modes with periods shorter than T_{baseline} have already been detected through previous monitoring. However, this contradicts the fact that there have been no cases where the periodicity of rotational period variations has been definitively confirmed, even for CU Vir. Consequently, magnetic field structures that have such modes can be rejected. On the other hand, field structures with longer periods than T_{baseline} are allowed observationally. In the figure, this condition is represented with a gray or white background. Based on this condition, it is concluded that centrally concentrated magnetic field structures with a negative $n_{\text{B,rad}}$ is rejected for all magnetic stars.

Although not yet settled, changes in the sign of rotational period variations have been detected for V901 Ori, V913 Sco, and CU Vir, and these changes allow for the estimation of the variation periods. These values are represented by yellow horizontal dashed lines in the figure. Our theoretical model, with its strong dependency on $n_{\text{B,rad}}$, allows for explanations of a wide range of the value. As a consequence, the periods for these stars can be explained by setting $n_{\text{B,rad}} \gtrsim 1.0$. This might suggest that the magnetic field structure inside the stars is strong near the surface.

4. Discussion

4.1. Limitations of our model

In our framework, a key assumption for one-dimensionalization is the shellular rotation law, where the material at the same radius (originally on an isopressure surface) is assumed to have the same angular velocity. This assumption may be justified if structural changes occur on the timescale of stellar evolution, since it is sufficiently long, allowing turbulent viscosity originating from horizontal turbulence to relax the angular momentum distribution. However, it is uncertain whether the same process occurs on the Alfvén time that is much shorter than the evolutionary timescale. Instead, one might consider that differential rotation develops in the horizontal direction during the propagation of Alfvén waves.

Without assuming shellular rotation, Alfvén waves traveling along different magnetic field lines would have distinct crossing times. In this case, differential rotation between gas associated with adjacent magnetic field lines may induce turbulence, causing phase mixing (cf, Charbonneau & MacGregor 1992, 1993). To determine oscillation periods of stationary Alfvén waves in this context, a two-dimensional linear analysis, considering the efficiency of phase mixing, will be suitable.

Taking this into account, in the current one-dimensional framework, the model's accuracy is expected to decrease as the crossing time for each magnetic field line becomes different. Figure 2 suggests that in centrally concentrated magnetic field structures ($n \lesssim 0$), where path lengths are close, the model's accuracy might not be severely affected. Conversely, in surface-concentrated magnetic field structures ($n \gtrsim 0$), there could be a potential mismatch between the predictions of our one-dimensional model and future two-dimensional models.

Another influential simplification is our assumption that the rotation and the magnetic axes are aligned. In reality, it is common for the two axes not to align, so that analyses using the Oblique Rotator Model are commonly conducted. However, our analysis has also shown that the period of rotational period variations is simply determined by the Alfvén wave crossing time. Therefore, even when considering the obliquity, we expect only a few-fold difference in the variation periods, which is unlikely to affect the conclusions of this study.

In upper main sequence stars, a strong dynamo-generated magnetic field may exist within the convective core (e.g., Featherstone et al. 2009; Augustson et al. 2016). Dynamo-driven fields may show reversals of their polarity. It is thus reasonable to assume that the dynamo-generated field is not directly connected to the stable magnetic field in the radiative layer. In a one-dimensional model, this disconnection may be represented by setting the magnetic field strength to zero at the boundary of the convective region. However, in our approach, the zero magnetic field causes the local crossing time to diverge, making it complicated to estimate the crossing time. Due to this issue, applying our model to cases with strong dynamo fields remains challenging. However, the radius of the convective core region is relatively small, and its crossing time is not expected to dominate over the crossing time of the outer radiative layers. Therefore, our current analysis is expected to provide a reasonable order of magnitude estimate of the oscillation period.

4.2. Comparison with Krtićka's model

Krtićka et al. (2017) also analyzed the rotational period variations of CU Vir and V901 Ori based on the picture that the

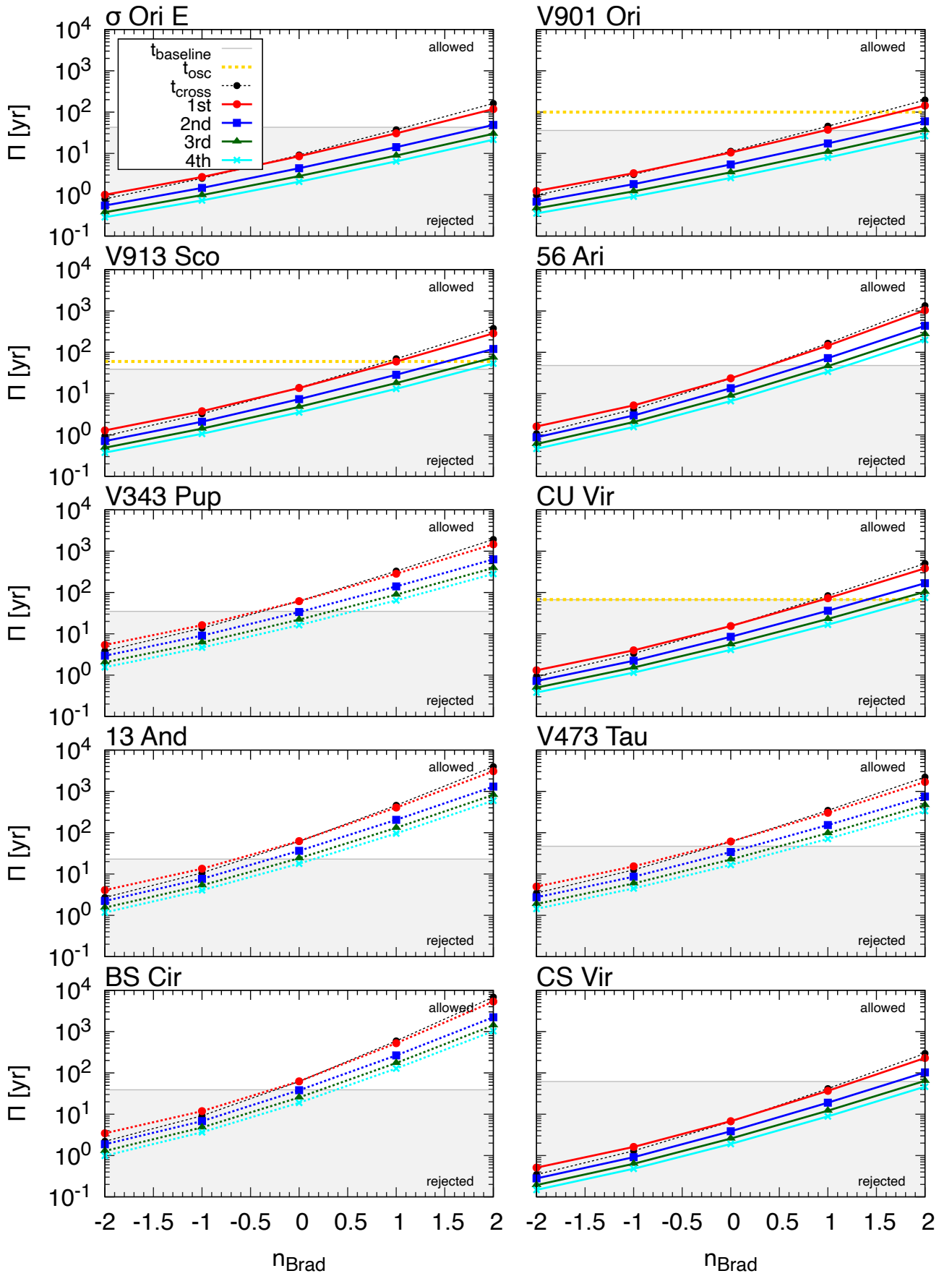


Fig. 7. The same as Fig. 4, but for all the magnetic stars where rotational period variations have been observed.

variations are induced by standing Alfvén waves. The one-dimensional magnetohydrodynamic equations they obtained are similar to ours, but they use a different poloidal magnetic field configuration that is expressed in the (R, Z) plane as

$$(B_R, B_Z) = \left(B, -\frac{zB}{R} \right), \quad (9)$$

where B is a constant. Their model yielded oscillation periods of 51 years for CU Vir and 5 years for V901 Ori. As a result, they concluded that the rotational period variation observed in CU Vir, with a period of approximately 70 years, can be explained by standing Alfvén waves. However, the variation in V901 Ori, estimated to have a period of over 100 years, cannot.

While dealing with similar models, our work has resulted in different conclusions. The main factor contributing to this difference is likely to be the different assumptions about the poloidal magnetic field structure. As demonstrated earlier, our model can alter the period of standing Alfvén waves by several orders of magnitude by changing the radial dependence of the poloidal magnetic field. On the other hand, it can be inferred that Krticka’s model, which has only tested a single field structure, had a limited range of explainable periods. Regarding the surface magnetic field, Krticka applied $B_p = 10$ kG, given the highly complex surface magnetic field structure. In contrast, we employed a dipole component of 6.1 kG obtained from Shultz et al. (2019b). While using a weaker value results in longer oscillation periods, the effect is considered minor, at most doubling the period.

4.3. Estimating the magnetic field structure based on the rotational period variation

Centrally concentrated magnetic fields appear unlikely based on the lack of detected oscillations in most stars. If they were, Alfvén waves would rather quickly pass through the entire star, resulting in a sufficiently short period of the rotational period variation to be detected. Comparison with three stars that potentially show cyclic variations (V901 Ori, CU Vir, and V913 Sco) suggests that the degree of surface concentration of the internal poloidal field is moderate ($n_{B_{\text{rad}}} \sim +1$).

The geometry of magnetic fields in equilibrium in the stellar interior has been investigated with MHD simulation (e.g., Braithwaite & Spruit 2004; Becerra et al. 2022) and with analytical approaches (e.g., Lyutikov 2010; Duez & Mathis 2010; Akgün et al. 2013). The surface-concentrated magnetic field structures as described in our model ($n_{B_{\text{rad}}} > 0$) resemble the equilibrium structures obtained numerically (Braithwaite & Spruit 2004) more than the central-concentrated structure ($n_{B_{\text{rad}}} < 0$).

If the estimates of surface concentration for the three stars that show cyclic variations were quantitatively accurate, the most massive of them, V901 Ori, exhibits the strongest surface concentration ($n_{B_{\text{rad}}} \sim +1.7$), suggesting that the degree of surface concentration may correlate with the mass of the stars. Another possibility is that, considering that the age of V901 Ori is almost zero while the fractional MS ages of V913 Sco and CU Vir are in the range of 0.1–0.3, the initially more surface-concentrated magnetic field would permeate deeper into the star as it evolves. There are indications that the magnetic field structure of magnetic stars becomes simplified with age (Rusomarov et al. 2015; Silvester et al. 2015). It is also possible that such global evolution is occurring simultaneously within the stellar interior. However, this evolutionary scenario may contradict the results of Braithwaite & Nordlund (2006), where the poloidal field stabilized by

the toroidal field rises to the surface due to magnetic diffusion over time, weakening the magnetic field strength near the center.

Our analysis is limited by the small sample size and the simple quantification methods. Additionally, V901 Ori is known to have a highly complex surface magnetic field structure (Kochukhov et al. 2010), unlike the largely dipolar magnetic fields of CU Vir (Kochukhov et al. 2014) and V913 Sco (Shultz et al. 2019a). Further research is necessary to validate trends and dependencies related to the internal magnetic field.

4.4. Implications from strong magnetic fields detected in red giant stars

Li et al. (2023) reported that the shift in dipole mode frequency observed in red giants can be explained by a strong magnetic field of 20–150 kG above the H-burning shell. Applying the magnetic flux conservation to the radial distribution obtained from our 1.5 M_{\odot} model yields a magnetic field strength of approximately 0.5–5 kG at a mass coordinate of $\sim 0.2 M_{\odot}$ at the TAMS stage. Since $\sim 0.2 M_{\odot}$ is larger than the maximum mass of the convective core ($\sim 0.12 M_{\odot}$), this field strength can be interpreted as representing the strength of a fossil magnetic field in the radiative layer. Most of the stars in Li’s sample were likely normal non-magnetic stars during their main sequence phase, so their surface magnetic field was at most on the order of ~ 1 G. This means that the red giants analyzed by Li et al. had a centrally concentrated magnetic field during their main sequence phase, which contradicts our conclusions.

Li et al. provided an alternative interpretation for the origin of the frequency shift. Specifically, the kernel function used to estimate the frequency shift is also sensitive to the region inside the H-burning shell. The observed frequency shift can then be explained by a magnetic field of 200–300 kG in the former convective core region, which can be accounted for by a convective dynamo driven by hydrogen burning. Our results are more consistent with this latter interpretation. Hence, they lead to the conclusion that a convective dynamo operates during hydrogen burning, and the magnetic field it generates remains after the cease of the core convection and causes the frequency shift observed in red giants. It should be noted that the method we used in this study is agnostic regarding the magnetic field distribution inside the stellar convective core. Thus, we do not rule out the possibility that a strong magnetic field, which is likely disconnected from the radiative layer, exists within the convective core.

Main sequence stars with masses less than around 1 M_{\odot} are considered to form radiative cores (Kippenhahn & Weigert 1990). Even in such low-mass stars, it is predicted that a small convective core forms due to non-equilibrium hydrogen burning mediated by ^3He and ^{12}C occurring just before the star enters the ZAMS. However, it is uncertain whether such a short-lived convective core can efficiently drive a dynamo, and if it can, whether the magnetic field will survive without dissipating during the long main sequence phase that follows. Hence, it is less likely that low-mass red giants possess strong internal magnetic fields similar to those of higher-mass red giants.

Therefore, the most direct way to determine the origin of the frequency shift will be to investigate whether similar shifts are seen in the low-mass red giants. Considering the inverse correlation between age and mass, finding and analyzing low-mass red giants may be less feasible, and the least massive star in the sample by Li et al. is estimated to have a mass of about 1.04 solar masses. Nevertheless, the Kepler targets include a non-negligible number of low-mass red giants (e.g., Yu et al. 2018). Investigat-

ing older, less massive red giants could shed light on this question.

4.5. Excitation mechanisms of standing Alfvén waves in magnetic AB stars

Magneto-sonic oscillations are thought to exist in magnetars, as signified by the quasi-periodic oscillations in the tail of giant X-ray flares (e.g., Strohmayer & Watts 2005), as the oscillation frequency is well reproduced by global MHD simulations (Glampedakis et al. 2006; Gabler et al. 2018). In this case, fractures in the crust of the magnetar are thought to disturb the hydrostatic equilibrium, which can provide the excitation of the MHD waves.

It is not known what could excite Alfvén waves in magnetic main sequence stars. Since the ages of the investigated magnetic stars span several to a few hundred Myrs, which corresponds to $10^5 \dots 10^7$ oscillation periods, it appears unlikely that an event relating to the formation of these stars excited oscillations that are still ongoing. On the other hand, the nuclear evolution of the considered main sequence stars imposes changes in the rotation period of the order of $10^{-10} \text{ s s}^{-1}$, which is comparable to the observed period variations of $10^{-2} \text{ s yr}^{-1} \sim 3 \times 10^{-10} \text{ s s}^{-1}$. Given these rough estimates, it may appear possible that the observed period changes are produced by standing Alfvén waves driven by changes in the internal shear layers on the nuclear timescale.

Furthermore, coupling between the core convection and the envelope magnetic field could excite magneto-sonic waves. Indeed, for red giant stars, Lecoanet et al. (2017) found that internal gravity waves can be efficiently converted into magnetic waves under certain conditions. Finally, Krtićka et al. (2017) suggested that coupling of a stellar wind with the stellar magnetosphere could excite Alfvén waves. While sufficiently strong winds are not predicted for late B and A type stars, their presence is suggested for CU Vir based on its periodic radio emission (Trigilio et al. 2000).

4.6. Towards future detections of rotational period variations

If we assume that the typical surface concentration of the magnetic field resembles our case $n_{\text{B,rad}} \sim +1$, the period of cyclic variations is expected to inversely correlate with the strength of the surface magnetic field (eq.7) and to show an increasing correlation with age and a decreasing correlation with mass (Fig. 5). Based on these trends, it would be possible to devise strategies to discover new stars exhibiting rotational period variations, and even more, cyclic variations.

Among the ten magnetic stars analyzed in this study, most of those with known surface field strength have observational baselines comparable to the predicted periods for the case $n_{\text{B,rad}} = +1$. Within the next few decades, it may be possible that the second time derivative of the rotation period will be measured in these stars. 56 Ari has an exceptionally short observational baseline compared to the $n_{\text{B,rad}} = +1$ period, which may suggest that the rotational period variations of this star are not due to the Alfvén wave but rather due to precession (Shore & Adelman 1976; Adelman & Fried 1991). Determinations of the rotational period for this star have not been reported since 2001 to our knowledge. The passage of more than 20 years will aid in the detection of the second derivative component of rotational period variations, which is essential for constraining models.

For stars without constraints on surface magnetic fields, we estimate the $n_{\text{B,rad}} = +1$ periods for a typical field strength of 1

kG, and their values are generally one order of magnitude larger than observational baselines. The difference in timescales suggests that these stars may have relatively strong surface magnetic fields, around 10 kG. Alternatively, they could possess relatively centrally concentrated internal magnetic fields ($n_{\text{B,rad}} \sim +0$). If the surface magnetic fields of these stars were weaker, around 100 G, it might contradict the idea that rotational period variations are due to Alfvén waves, suggesting instead that they are caused by precession. Hence, when magnetic stars exhibiting variations of the rotational period are discovered, it is crucial to estimate the surface magnetic field strength through spectropolarimetric observations.

Until now, the detection of rotational period variations has been biased towards rapidly rotating stars with rotation periods of around one day. This is because a shorter rotation period makes it easier to meet the condition of observing as many cycles of rotation as possible, which is required for detecting rotational period variations (Pyper & Adelman 2020). However, such rapidly rotating magnetic stars are biased towards younger stars (Fossati et al. 2016; Shultz et al. 2018; Keszthelyi et al. 2020), and it is known that the majority of magnetic stars have longer rotation periods, peaking around three days (Kochukhov & Bagnulo 2006; Netopil et al. 2017). It is important to search for rotational period variations in the more common magnetic stars with longer rotation periods and relatively older ages.

Another factor, the amplitude, is preferable to be large for the detection of rotational period variation. In this study, linear analysis is conducted so that the investigation of the amplitude is not feasible. To do so, further research is needed on how the rotational period variation is driven and to what extent the long-term growth and dissipation occur.

5. Concluding remarks

In this paper, we explore the existence and properties of torsional Alfvén waves in magnetic stars on the upper main sequence. Based on the concepts developed in Takahashi & Langer (2021), we perform an eigenmode analysis of standing Alfvén waves in such stars and derive the most likely oscillation frequencies. We do this while assuming different degrees of the central- or surface-concentration of the magnetic field, which results in largely different frequencies.

We compare our results with the rate of change of the stellar rotation period, and find, as Krtićka et al. (2017), that they can be compatible with the periods of the standing Alfvén waves. However, our results imply compatibility only for the case that the magnetic fields in these stars are concentrated towards the stellar surface, and outline the potential of this type of technique to explore the properties of the magnetic field in stellar envelopes.

Acknowledgements. K.T. thanks to Kengo Tomida and Fabian Schneider for fruitful discussions. This work was supported in part by JSPS KAKENHI Grant Numbers JP22K20377, JP24K17102.

References

- Adelman, S. J., Dukes, Robert J., J., & Pyper, D. M. 1992, *AJ*, 104, 314
- Adelman, S. J. & Fried, R. E. 1991, *International Amateur-Professional Photometric Photometry Communications*, 45, 4
- Adelman, S. J., Malanushenko, V., Ryabchikova, T. A., & Savanov, I. 2001, *A&A*, 375, 982
- Akgün, T., Reisenegger, A., Mastrano, A., & Marchant, P. 2013, *Monthly Notices of the Royal Astronomical Society*, 433, 2445
- Augustson, K. C., Brun, A. S., & Toomre, J. 2016, *The Astrophysical Journal*, 829, 92

- Babcock, H. W. 1947a, *PASP*, 59, 260
 Babcock, H. W. 1947b, *ApJ*, 105, 105
 Babcock, H. W. 1948, *PASP*, 60, 245
 Babcock, H. W. 1949, *The Observatory*, 69, 191
 Babcock, H. W. 1958, *ApJS*, 3, 141
 Becerra, L., Reisenegger, A., Valdivia, J. A., & Gusakov, M. 2022, *MNRAS*, 517, 560
 Beck, P. G., De Ridder, J., Aerts, C., et al. 2012, *Astronomische Nachrichten*, 333, 967
 Belopolsky, A. 1913, *Astronomische Nachrichten*, 196, 1
 Braithwaite, J. & Nordlund, Å. 2006, *A&A*, 450, 1077
 Braithwaite, J. & Spruit, H. C. 2004, *Nature*, 431, 819
 Braithwaite, J. & Spruit, H. C. 2017, *Royal Society Open Science*, 4, 160271
 Cantat-Gaudin, T., Mapelli, M., Balaguer-Núñez, L., et al. 2019, *A&A*, 621, A115
 Charbonneau, P. & MacGregor, K. B. 1992, *ApJ*, 387, 639
 Charbonneau, P. & MacGregor, K. B. 1993, *ApJ*, 417, 762
 Cox, A. N. 2000, *Allen's astrophysical quantities*
 Deheuvels, S., Doğan, G., Goupil, M. J., et al. 2014, *A&A*, 564, A27
 Deutsch, A. J. 1947, *ApJ*, 105, 283
 Deutsch, A. J. 1954, *Transactions of the International Astronomical Union*, 8, 801
 Deutsch, A. J. 1958, in *Electromagnetic Phenomena in Cosmical Physics*, ed. B. Lehnert, Vol. 6, 209
 Duez, V. & Mathis, S. 2010, *A&A*, 517, A58
 Esplin, T. L., Luhman, K. L., Miller, E. B., & Mamajek, E. E. 2018, *AJ*, 156, 75
 Featherstone, N. A., Browning, M. K., Brun, A. S., & Toomre, J. 2009, *ApJ*, 705, 1000
 Feiden, G. A. & Chaboyer, B. 2012, *ApJ*, 761, 30
 Feiden, G. A. & Chaboyer, B. 2013, *ApJ*, 779, 183
 Feiden, G. A. & Chaboyer, B. 2014, *ApJ*, 789, 53
 Ferrario, L. & Wickramasinghe, D. 2006, *Monthly Notices of the Royal Astronomical Society*, 367, 1323
 Fossati, L., Schneider, F. R. N., Castro, N., et al. 2016, *A&A*, 592, A84
 Fuller, J., Cantiello, M., Stello, D., Garcia, R. A., & Bildsten, L. 2015, *Science*, 350, 423
 Fuller, J., Piro, A. L., & Jermyn, A. S. 2019, *MNRAS*, 485, 3661
 Gabler, M., Cerdá-Durán, P., Stergioulas, N., Font, J. A., & Müller, E. 2018, *MNRAS*, 476, 4199
 Georgy, C., Meynet, G., Ekström, S., et al. 2017, *A&A*, 599, L5
 Glampedakis, K., Samuelsson, L., & Andersson, N. 2006, *MNRAS*, 371, L74
 Griffiths, A., Eggenberger, P., Meynet, G., Moyano, F., & Aloy, M.-Á. 2022, *A&A*, 665, A147
 Guthnick, P. & Prager, R. 1914, *Photoelektrische untersuchungen an spektroskopischen Doppelsternen und an Planeten*
 Heger, A., Langer, N., & Woosley, S. E. 2000, *ApJ*, 528, 368
 Heger, A., Woosley, S. E., & Spruit, H. C. 2005, *ApJ*, 626, 350
 Jeffries, R. D., Jackson, R. J., Franciosini, E., et al. 2017, *MNRAS*, 464, 1456
 Keszthelyi, Z. 2023, *Galaxies*, 11, 40
 Keszthelyi, Z., Meynet, G., Georgy, C., et al. 2019, *MNRAS*, 485, 5843
 Keszthelyi, Z., Meynet, G., Shultz, M. E., et al. 2020, *MNRAS*, 493, 518
 Kippenhahn, R. & Weigert, A. 1990, *Stellar Structure and Evolution*
 Kochukhov, O. & Bagnulo, S. 2006, *A&A*, 450, 763
 Kochukhov, O., Lüftinger, T., Neiner, C., Alecian, E., & MiMeS Collaboration. 2014, *A&A*, 565, A83
 Kochukhov, O., Lundin, A., Romanyuk, I., & Kudryavtsev, D. 2010, *The Astrophysical Journal*, 726, 24
 Krtićka, J., Mikulášek, Z., Henry, G. W., Kurfürst, P., & Karlický, M. 2017, *MNRAS*, 464, 933
 Landstreet, J. D. 1992, *A&A Rev.*, 4, 35
 Lecoanet, D., Bowman, D. M., & Van Reeth, T. 2022, *MNRAS*, 512, L16
 Lecoanet, D., Vasil, G. M., Fuller, J., Cantiello, M., & Burns, K. J. 2017, *MNRAS*, 466, 2181
 Li, G., Deheuvels, S., Ballot, J., & Lignières, F. 2022, *Nature*, 610, 43
 Li, G., Deheuvels, S., Li, T., Ballot, J., & Lignières, F. 2023, *A&A*, 680, A26
 Lockyer, N. & Baxandall, F. E. 1906, *Proceedings of the Royal Society of London Series A*, 77, 550
 Ludendorff, H. 1906, *Astronomische Nachrichten*, 173, 1
 Luhman, K. L. & Esplin, T. L. 2020, *AJ*, 160, 44
 Lyutikov, M. 2010, *MNRAS*, 402, 345
 Maeder, A. & Meynet, G. 2004, *A&A*, 422, 225
 Maury, A. C. & Pickering, E. C. 1897, *Annals of Harvard College Observatory*, 28, 1
 Meynet, G., Eggenberger, P., & Maeder, A. 2011, *A&A*, 525, L11
 Mikulášek, Z. 2016, *Contributions of the Astronomical Observatory Skalnaté Pleso*, 46, 95
 Mikulášek, Z., Krtićka, J., Henry, G. W., et al. 2011, *A&A*, 534, L5
 Mikulášek, Z., Krtićka, J., Henry, G. W., et al. 2008, *A&A*, 485, 585
 Mikulášek, Z., Semenko, E., Paunzen, E., et al. 2022, *A&A*, 668, A159
 Morgan, W. W. 1931, *ApJ*, 74, 24
 Morgan, W. W. 1933, *ApJ*, 77, 330
 Mosser, B., Goupil, M. J., Belkacem, K., et al. 2012, *A&A*, 548, A10
 Netopil, M., Paunzen, E., Hümmerich, S., & Bernhard, K. 2017, *MNRAS*, 468, 2745
 Oksala, M. E., Kochukhov, O., Krtićka, J., et al. 2015, *MNRAS*, 451, 2015
 Ozuyar, D., Sener, H. T., & Stevens, I. R. 2018, *Publications of the Astronomical Society of Australia*, 35, e004
 Ozuyar, D. & Stevens, I. R. 2018, *Information Bulletin on Variable Stars*, 6245, 1
 Petermann, I., Langer, N., Castro, N., & Fossati, L. 2015, *A&A*, 584, A54
 Petit, V., Keszthelyi, Z., MacInnis, R., et al. 2017, *MNRAS*, 466, 1052
 Pinsonneault, M. H., Kawaler, S. D., Sofia, S., & Demarque, P. 1989, *ApJ*, 338, 424
 Potter, A. T., Chitre, S. M., & Tout, C. A. 2012, *MNRAS*, 424, 2358
 Preston, G. W. 1974, *ARA&A*, 12, 257
 Prisinzano, L., Damiani, F., Micela, G., et al. 2016, *A&A*, 589, A70
 Pyper, D. M. & Adelman, S. J. 2020, *PASP*, 132, 024201
 Pyper, D. M. & Adelman, S. J. 2021, *PASP*, 133, 084203
 Pyper, D. M., Ryabchikova, T., Malanushenko, V., et al. 1998, *A&A*, 339, 822
 Reiners, A., Stahl, O., Wolf, B., Kaufer, A., & Rivinius, T. 2000, *A&A*, 363, 585
 Román-Zúñiga, C. G., Kounkel, M., Hernández, J., et al. 2023, *AJ*, 165, 51
 Rusomarov, N., Kochukhov, O., Ryabchikova, T., & Piskunov, N. 2015, *A&A*, 573, A123
 Shore, S. N. & Adelman, S. J. 1976, *ApJ*, 209, 816
 Shultz, M., Rivinius, T., Das, B., Wade, G. A., & Chand ra, P. 2019a, *MNRAS*, 486, 5558
 Shultz, M. E., Owocki, S. P., ud-Doula, A., et al. 2022, *MNRAS*, 513, 1429
 Shultz, M. E., Wade, G. A., Rivinius, T., et al. 2019b, *MNRAS*, 490, 274
 Shultz, M. E., Wade, G. A., Rivinius, T., et al. 2018, *MNRAS*, 475, 5144
 Silvester, J., Kochukhov, O., & Wade, G. A. 2015, *MNRAS*, 453, 2163
 Spruit, H. C. 1999, *A&A*, 349, 189
 Spruit, H. C. 2002, *A&A*, 381, 923
 Stępień, K. 1998, *A&A*, 337, 754
 Stello, D., Cantiello, M., Fuller, J., et al. 2016, *Nature*, 529, 364
 Stibbs, D. W. N. 1950, *MNRAS*, 110, 395
 Strohmayer, T. E. & Watts, A. L. 2005, *ApJ*, 632, L111
 Takahashi, K. & Langer, N. 2021, *A&A*, 646, A19
 Tarricq, Y., Soubiran, C., Casamiquela, L., et al. 2021, *A&A*, 647, A19
 Townsend, R. H. D., Oksala, M. E., Cohen, D. H., Owocki, S. P., & ud-Doula, A. 2010, *ApJ*, 714, L318
 Triglio, C., Leto, P., Leone, F., Umana, G., & Buemi, C. 2000, *A&A*, 362, 281
 Wade, G. A., Grunhut, J., Alecian, E., et al. 2014, in *IAU Symposium*, Vol. 302, *Magnetic Fields throughout Stellar Evolution*, ed. P. Petit, M. Jardine, & H. C. Spruit, 265–269
 Weber, E. J. & Davis, Leverett, J. 1967, *ApJ*, 148, 217
 Wheeler, J. C., Kagan, D., & Chatzopoulos, E. 2015, *ApJ*, 799, 85
 Wolff, S. C. 1983, *The A-type stars: problems and perspectives*.
 Yu, J., Huber, D., Bedding, T. R., et al. 2018, *ApJS*, 236, 42
 Zahn, J.-P. 1992, *A&A*, 265, 115
 Zapatero Osorio, M. R., Béjar, V. J. S., Pavlenko, Y., et al. 2002, *A&A*, 384, 937
 Ziznovsky, J., Schwartz, P., & Zverko, J. 2000, *Information Bulletin on Variable Stars*, 4835, 1